

A methodology, based on sintering-induced stiffening, for prediction of the spallation lifetime of plasma-sprayed coatings

M. Shinozaki, T.W. Clyne*

Department of Materials Science & Metallurgy, Cambridge University, Pembroke Street, Cambridge CB2 3QZ, UK

Received 4 September 2012; received in revised form 26 September 2012; accepted 29 September 2012

Available online 6 November 2012

Abstract

This study concerns the effect of sintering-induced stiffening in promoting spallation of plasma-sprayed yttria-stabilized zirconia thermal barrier coatings. Coatings with thickness in the range 350–800 μm were sprayed onto dense alumina substrates. In order to ensure a tough interface, the surface of the alumina substrates were first roughened by laser treatment. Specimens were heat treated at 1500 $^{\circ}\text{C}$ and periodically quenched to ~ 100 $^{\circ}\text{C}$, using nitrogen jets. During cooling, specimens were monitored for spallation via a webcam. Spallation lifetimes were observed to be shorter for thicker coatings. Using a simple fracture mechanics approach, with the strain energy release rate obtained using measured coating stiffness values, the behaviour was found to be consistent with an approximately constant interfacial fracture energy value of the order of 300 J m^{-2} . If this interfacial toughness had been known beforehand, then the rationale presented here could have been used for prediction of coating lifetime. While the experiments are based on use of a ceramic substrate, the approach could be applied to conventional metallic substrate systems.

© 2012 Acta Materialia Inc. Published by Elsevier Ltd. All rights reserved.

Keywords: Thermal barrier coating (TBC); Yttria-stabilized zirconia (YSZ); Plasma spraying; Spallation; Sintering

1. Introduction

Thermal barrier coatings (TBCs) are widely used in turbines designed for propulsion or power generation [1–7]. They comprise insulating ceramic material, commonly yttria-stabilized zirconia (YSZ), deposited onto a metallic component, often with a bond coat of some sort. The YSZ layer provides thermal insulation, creating temperature drops [7] in service of up to ~ 200 $^{\circ}\text{C}$ across a coating several hundred microns in thickness. The function of the bond coat is to provide improved adhesion and to act as an oxidation barrier, by developing a protective oxide layer (a thermally grown oxide, TGO), often consisting predominantly of $\alpha\text{-Al}_2\text{O}_3$. Improved TBC performance offers potential for improved component durability and for efficiency gains resulting from higher turbine entry temperatures and/or reduced cooling air requirements. However,

such efficiency gains can only be achieved if there can be a large measure of confidence in the thermo-mechanical stability of the TBC under service conditions.

The two main methods of TBC deposition are plasma spraying (PS) and electron beam physical vapour deposition. The focus of the current study is on PS TBCs, although it is expected that the conclusions will also apply to other types of coating. The microstructure of PS TBCs is composed of overlapping splats lying parallel to the substrate, with inter-lamellar pores, through-thickness intra-splat cracks and globular voids (see Fig. 1a). Plasma-sprayed TBCs have a low through-thickness thermal conductivity ($k \sim 0.5\text{--}1.0$ $\text{W m}^{-1} \text{K}^{-1}$) and a low global in-plane stiffness ($E \sim 10\text{--}20$ GPa) in the as-sprayed state. The low stiffness is beneficial in accommodating strains arising (during thermal cycling) from the mismatch in thermal expansivity between the TBC ($\alpha_{\text{TBC}} \sim 1.1 \times 10^{-5}$ K^{-1}) and the substrate ($\alpha_{\text{sub}} \sim 1.5 \times 10^{-5}$ K^{-1}). However, with extended exposure to high temperatures, there is a tendency for the TBC to undergo sintering, leading to increases in both thermal

* Corresponding author. Tel.: +44 1223 334332; fax: +44 1223 334567.
E-mail address: twc10@cam.ac.uk (T.W. Clyne).

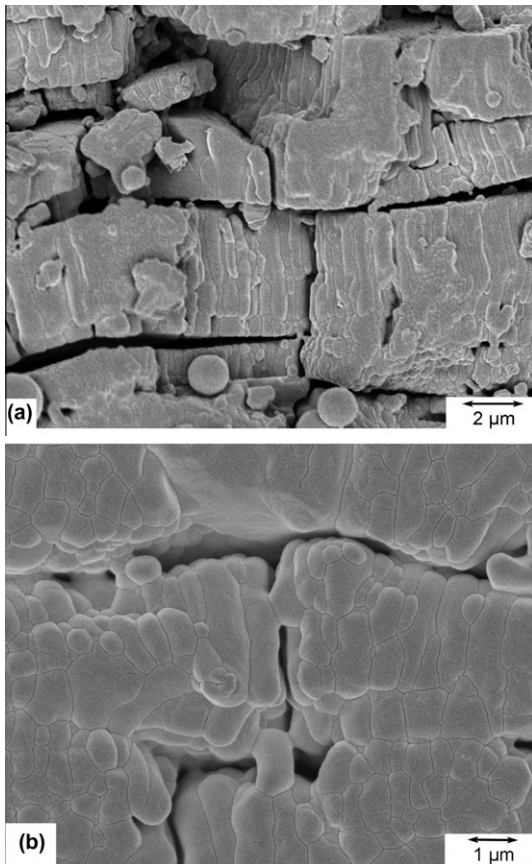


Fig. 1. SEM fracture surfaces, taken from Paul et al. [52], showing splat structures in PS YSZ coatings (a) as-sprayed and (b) after 10 h at 1400 °C.

conductivity [8,9] and stiffness [10–15]. The former is related to the growth of the inter-splat contact area [16], whilst the latter is associated with inter-splat locking and splat stiffening (see Fig. 1b).

Cipitria et al. [17,18] developed a sintering model that enables prediction of microstructural changes in terms of shrinkage, surface area and porosity. Analytical and numerical models simulating heat transfer through the TBC (allowing the effective thermal conductivity to be predicted as a function of microstructural parameters) can also be found in the literature [19,20]. Modelling of increases in stiffness due to sintering has not yet been undertaken, but it is well established that such stiffening can be pronounced and can promote spallation. It is also clear that these effects can be accelerated by the presence of calcia–magnesia–alumina–silica (CMAS) compounds [21–26], which can be ingested in the form of sand, fly ash, volcanic ash, etc.

The current paper utilizes a global fracture mechanics approach, focusing on the strain energy release rate arising from differential thermal contraction stresses (in the coating) and comparing this value with the interfacial fracture energy. When this strain energy release rate exceeds the fracture energy, then debonding (propagation of an interfacial crack) becomes energetically favourable and is hence likely to occur (provided such cracks can initiate, which

will depend on the presence of flaws, edge effects, etc.). This is, of course, not a new concept, and it has been applied to the debonding of YSZ coatings by a number of researchers [27–32]. However, the focus of much work on spallation has been on interfacial embrittlement [3,31–33], commonly associated with growth of the TGO at the interface, rather than on progressive increase of the driving force. Moreover, several workers [32,34] have regarded the driving force as strain energy stored in the TGO, rather than in the coating (top coat). Such an approach cannot account for experimental observations of thicker top coats debonding more readily than thin ones [29,35,36], or, indeed, that debonding is more likely when the top coat is stiffer [36–39]. Furthermore, since the TGO is very thin ($< \sim 10 \mu\text{m}$), a prediction that it can store strain energies sufficient to drive interfacial cracking requires the assumption that unrealistically high stress levels (in the GPa range) can be sustained within them. In practice, spallation commonly occurs as a result of sintering-induced stiffening throughout the top coat, although the interfacial toughness may simultaneously fall during prolonged exposure to high temperature – for example, as a consequence of TGO growth. There have been several studies [40–44] aimed at measuring the interfacial fracture energy, using a variety of techniques. These have mostly yielded values of the order of $50\text{--}150 \text{ J m}^{-2}$, with a tendency towards lower values in this range after prolonged heating.

In the work presented here, the details of the fracture mechanics analysis being proposed are clarified and then experimental work is described involving an alumina substrate, thus eliminating the complications that tend to arise from through-thickness thermal gradients and changes to the interfacial structure, and allowing the underlying premise of the model to be systematically tested (for the first time).

2. Experimental procedures

2.1. Background

The thermal stress, assumed to be equal biaxial (and taking through-thickness stresses to be negligible throughout), tends to be confined predominantly to the TBC (taken to be transversely isotropic and to exhibit linear elastic behaviour), since the substrate is appreciably thicker and stiffer. In other words, the thermal misfit strain between substrate and coating is accommodated almost entirely within the coating. It is assumed that the system is stress-free at the operating temperature – the creep behaviour of YSZ in this temperature range is such as to ensure that this condition is rapidly established [17,18]. After cooling from this temperature (T_2) to some lower temperature (T_1), which could be close to ambient, the (in-plane) stress created in the coating is given by [45]

$$\Delta\sigma = \frac{E_{\text{TBC}} \int_{T_1}^{T_2} (\alpha_{\text{sub}}(T) - \alpha_{\text{TBC}}(T)) dT}{1 - \nu} = \frac{E_{\text{TBC}}(\Delta\alpha\Delta T)}{1 - \nu} \quad (1)$$

Table 1

Approximate values [3,49,50] for the expansivities of alumina, YSZ and a typical Ni-based superalloy, and corresponding misfit strains for YSZ coatings on alumina and superalloy substrates, arising from a temperature drop of 1000 K.

Material	Thermal expansivity α (K^{-1})	Misfit strain from ΔT of $-1000 \text{ K} \Delta\alpha \Delta T$ (millistrain)
Alumina	$\sim 7\text{--}8 \times 10^{-6}$	~ 3.5
YSZ	$\sim 1.1 \times 10^{-5}$	~ 4
Superalloy	$\sim 1.4\text{--}1.6 \times 10^{-5}$	~ 4

where α_{sub} and α_{TBC} are the thermal expansivities of substrate and TBC and ν is the Poisson ratio of the TBC, taken in the present work to have a value of ~ 0.2 . The (interfacial) strain energy release rate for debonding of such a stressed coating is obtained by considering the relaxation of in-plane stresses during propagation of an interfacial crack, leading to [46]:

$$G_i = \frac{E_{\text{TBC}} h (\Delta\alpha \Delta T)^2}{2(1 - \nu)} \quad (2)$$

where h is the coating thickness. (This expression is based on the assumption that only the stress parallel to the direction of crack propagation is relaxed by the debonding, since the other in-plane stress is still constrained as the interfacial crack passes the region concerned.) It is assumed that spallation occurs when G_i reaches the critical value G_{ic} (the interfacial fracture energy). Equivalently, an observed spallation event (and the value of E_{TBC} at that point) can be used to evaluate G_{ic} . It may be noted that cracks propagating under this type of driving force will be doing so under predominantly mode II (shearing mode) loading. The appropriate fracture energy value will therefore be that for mode II, which will tend to be appreciably higher than the value for the same interface under mode I (opening mode) conditions [47,48].

Experimental work in the current study involves alumina substrates. Use of this material ensured that there was little or no degradation of the substrate or the interface during (isothermal) heat treatments, even at temperatures as high as 1500 °C. It should be noted that the misfit strain ($\Delta\alpha\Delta T$) in this system has the opposite sign to that in a more conventional (zirconia/superalloy) coating/substrate combination, since alumina has a lower thermal expansivity than zirconia. The coating stress is thus tensile after cooling (from a stress-free upper temperature), whereas it is compressive for a conventional system. However, since only the square of this strain appears in Eq. (2), the driving force for interfacial debonding is unaffected by its sign. As can be seen from the data [3,49,50] in Table 1, the magni-

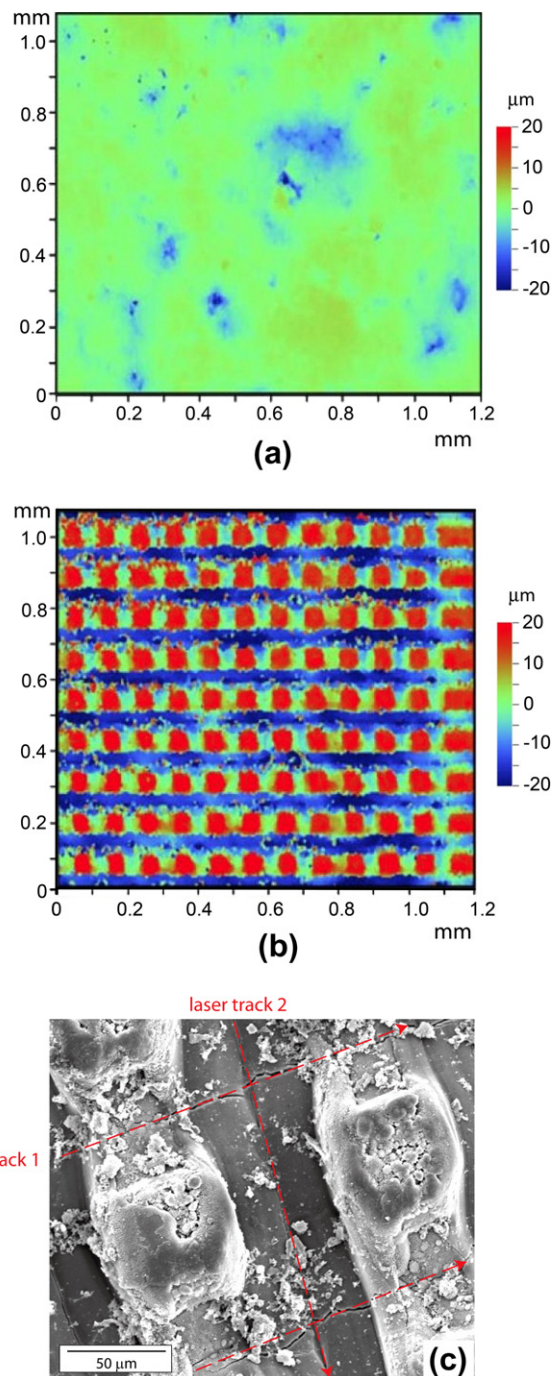


Fig. 2. Illustration of the topography of alumina substrates, in the form of optical interferometric surface height maps (a) before and (b) after laser treatment, and (c) SEM image showing the relation between topographic features and laser tracks.

tude of the driving force, for a given temperature drop, is similar for zirconia/superalloy and zirconia/alumina combinations.

Table 2

Laser processing parameters for surface treatment of alumina substrates.

Power (W)	Frequency (kHz)	Feed rate (mm s^{-1})	Pulse length (μs)	Number of scans	Track spacing (μm)
30	75	550	1200	5	100

Table 3
Composition of 204NS (Sulzer-Metco) powder.

Composition (wt.%)								
ZrO ₂	Y ₂ O ₃	HfO ₂	Al ₂ O ₃	SiO ₂	TiO ₂	CaO	MgO	Fe ₂ O ₃
Bal.	7.6	1.5	<0.01	0.07	0.09	<0.01	<0.01	<0.01

Table 4
Parameters used for plasma spraying of YSZ onto alumina substrates.

Spraying facility	F4 Plasma Technik VPS
Chamber pressure (mbar of Ar)	200
Nozzle diameter (mm)	8
Plasma gas flow rates (l min ⁻¹)	Ar 50, H ₂ 7
Carrier gas flow rates (l min ⁻¹)	Ar 3.5
Arc current (A)	760
Voltage (V)	50
Power (kW)	38
Preheat stand-off distance (mm)	400 (4 passes) 270 (2 passes)
Spraying stand-off distance (mm)	270

2.2. Alumina substrate laser treatment

In order to ensure good adhesion of the plasma-sprayed YSZ coating, the surface of the alumina substrates was roughened using a scanning laser beam. An SPI[®] 200 W water-cooled fibre laser (its active gain medium being an optical fibre doped with rare earth elements). The processing parameters are summarized in Table 2. The resultant topography of the alumina substrate is illustrated in Fig. 2, which presents both surface height maps (obtained using a WYKO RST Plus Optical Interferometer) and a scanning electron microscope (SEM) micrograph. The surface roughness (R_a), measured using a Veeco Dektak 6 M Stylus Profiler over a length of 5 mm, was observed to increase from $\sim 1.0 \mu\text{m}$ for the as-received substrates to $\sim 9.5 \mu\text{m}$ after laser treatment.

2.3. Plasma spraying

The YSZ coatings were produced in Cambridge by plasma spraying of a standard (Sulzer 204NS) powder, with the composition given in Table 3, using a Plasma-Technik VPS system with an F4 gun. The spray parameters are summarized in Table 4. (It is common for PS YSZ coatings to be produced in air – i.e. using APS – but it was found to be necessary to use VPS in order to ensure that the interfacial adhesion was adequate.) The alumina substrates were 5 mm thick, with in-plane dimensions of 50 mm \times 50 mm. The temperature of the reverse side of the substrates was monitored during spraying, using a thermocouple spot welded onto a metallic plate, which was cemented onto the back of the substrate. This temperature typically reached a maximum of about 600 °C by the end of the preheat passes. After spraying, specimens were cut using a diamond wheel, with a slow feed rate, giving dimensions of $\sim 13 \times 10 \times 5 \text{ mm}$.

2.4. Heat treatment, periodic quenching and spallation monitoring

A computer-controlled furnace with a periodic quenching capability (see Fig. 3a) was used to investigate coating spallation. The set-up comprises a tube furnace (Elite Thermal Systems, model TSH16), with a recrystallized alumina tube of diameter 50 mm. A motorized mechanism periodically pushes the sample boat in and out of the furnace. Each boat typically contained about six samples. When withdrawn, the samples were quenched with nitrogen gas jets. An R-type thermocouple was located inside the sample boat, to monitor their temperature. A typical specimen thermal history is shown in Fig. 3b, where it can be seen that the furnace temperature in this case was 1500 °C and quenching (to approximately 100 °C) took place at hourly intervals, induced by 5 min of exposure to the nitrogen jets. The system incorporates a webcam focused on the sample boat, the output of which is recorded during quenching. Inspection of recorded images allowed the time of spallation to be established for individual specimens, without the need for frequent personal inspection. In this way, it is practicable to obtain data relating to substantial numbers of specimens, exhibiting relatively long spallation lifetimes.

2.5. Measurement of coating expansivity and stiffness

Free-standing YSZ specimens were obtained by spraying (using the parameters in Table 3) onto grit-blasted mild steel substrates. Detachment from the substrates was achieved by immersion in 36% HCl, which caused partial dissolution of the steel. These specimens were used to determine the coating expansivity¹ and its stiffness (as a function of heat treatment time and temperature). Heat treatments were conducted in the periodic quenching furnace described in Section 2.4. Two specimen arrangements were employed, the YSZ samples being located on (2 mm thick) alumina plates either with or without a second (2 mm thick) alumina plate on top of them. This was done in view of observations that, particularly at very high temperatures (i.e. 1500 °C), there was a tendency in the absence of the second alumina plate for the coatings to become curved. Such curvature is prone to cause stiffness measurements obtained by bending tests (see below) to give over-estimated values.

¹ The thermal expansivity of a material is unaffected by the presence, level or distribution of porosity, so there was no need to repeat these measurements after different heat treatments.

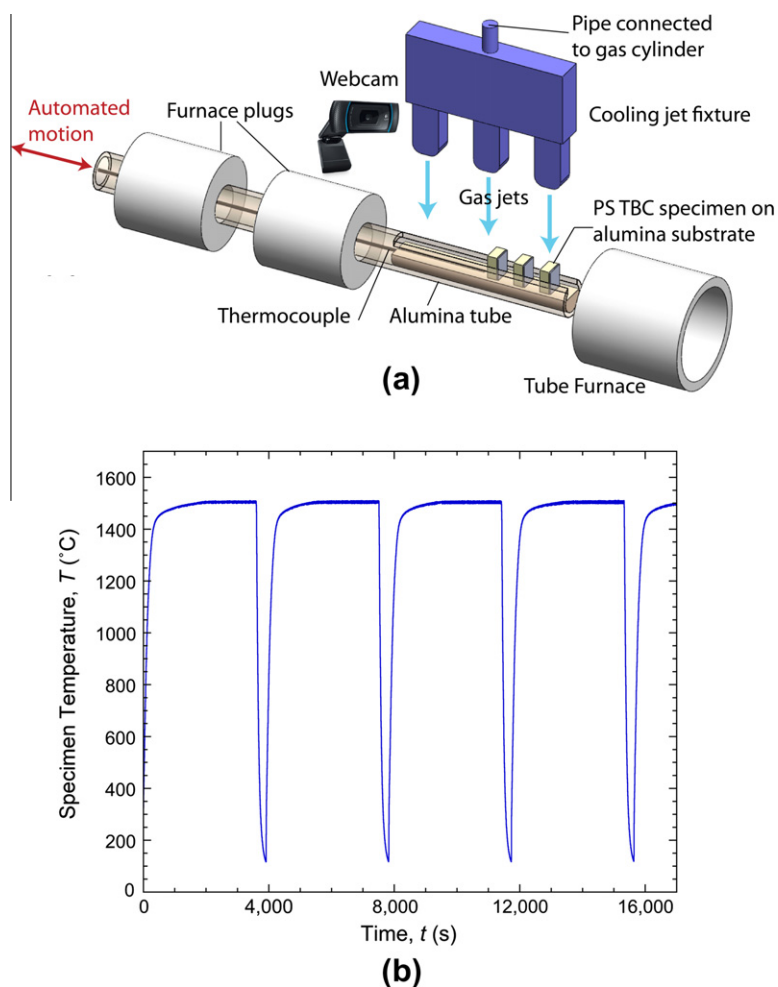


Fig. 3. Illustration of the periodic quenching system, showing (a) a schematic depiction and (b) a typical thermal history from the thermocouple located in the specimen boat.

Expansivity data for the YSZ coatings (and for the dense alumina substrates) were obtained using a Netzsch 402C dilatometer. The set-up comprises an alumina stage with an alumina push rod, which applies a constant load to the specimen (of 0.3 N). A linear variable displacement transducer measures the displacement of the push rod. Samples were heated and cooled between 20 and 1200 °C at 10 °C min⁻¹. A calibration run was conducted in order to correct for dimensional change of the alumina push rod.

In-plane Young's modulus values were obtained via four-point bending, using a scanning laser extensometer (Lasermike model 501-195, with a resolution of around 3 μm) to monitor specimen deflections. Specimen dimensions were approximately 12 × 40 × 0.4 mm. All measurements were made at room temperature. Loads were applied via a counter-balanced platen, using small pre-weighed masses. It may be noted that values obtained in bending are weighted equally by tensile and compressive responses. In fact, these are expected [51] to be similar for strains up to about 0.7%, after which the compressive value is likely to be higher as a consequence of the closure of through-thickness microcracks. The strains induced during stiffness measurement ranged up to about 0.1%.

2.6. Microstructural examination

Coating microstructures were examined using a JEOL-5800 SEM, with a typical accelerating voltage of 10 kV. Samples were sputter coated with gold (using an Emitech 330 facility), to prevent charging.

3. Thermal expansion and stiffness characteristics

3.1. Thermal expansion

Dilatometry data in the form of a plot of strain against temperature are shown in Fig. 4 for the alumina substrate and for the free-standing YSZ coating. It can be seen that the expansivity of the YSZ is appreciably higher than that of the alumina at low temperatures ($\Delta\alpha \sim 3.9 \times 10^{-6} \text{ K}^{-1}$), although the difference is less pronounced at high temperatures ($\Delta\alpha \sim 1.3 \times 10^{-6} \text{ K}^{-1}$). The focus here is on the misfit strain, $\Delta\alpha \Delta T$, where ΔT is the effective temperature change during quenching and the difference in expansivity between coating and substrate should be summed over this range. In the present work, ΔT was taken to be from 1100 to 100 °C, giving a misfit strain (obtained by integration of

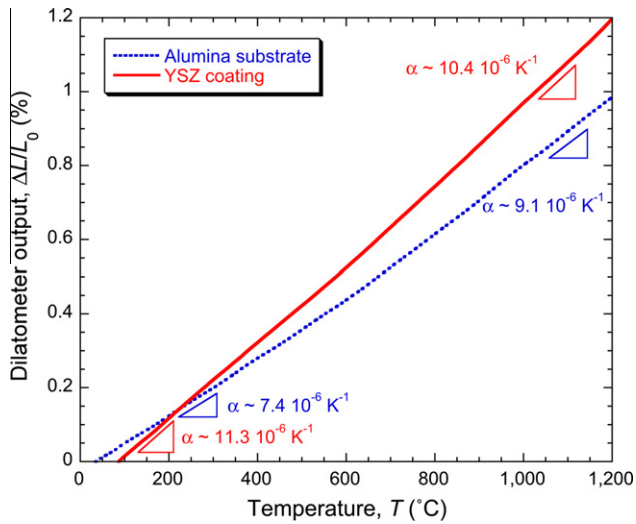


Fig. 4. Experimental dilatometry data, showing how the expansivities of the alumina substrate and the YSZ coatings vary with temperature.

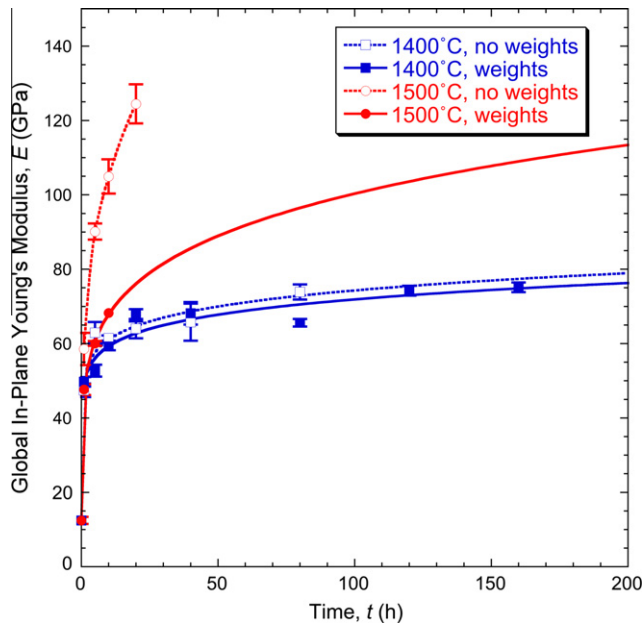


Fig. 5. Experimental stiffness data, obtained via four-point bending, for YSZ coatings heat treated at 1400 and 1500 °C.

$\Delta\alpha$ over this range) of approximately 2.2 millistrain. (The upper temperature was taken to be 1100 °C, rather than 1500 °C, in an attempt to take account of the substantial creep relaxation of stresses expected at temperatures above 1100 °C, which is likely to occur even with rapid cooling: this estimate is clearly a relatively crude one, although it is broadly based on information about creep rates obtained in the modelling work of Cipitria et al. [17,18].)

3.2. Sintering-induced stiffening

Fig. 5 shows measured Young's modulus values for free-standing YSZ coatings, as a function of heat treatment

time at 1400 and 1500 °C. These measurements were made with and without “weights” – i.e. an alumina plate on top of the specimen, which eliminated the development of curvature. The error bars represent standard deviations on sets of 2–4 specimens in each case.

The mechanisms of sintering operative in plasma-sprayed YSZ coatings are well established [17,18]. It can be seen in Fig. 5 that the associated stiffening is rapid at these very high temperatures. (In fact, even at temperatures as low as 1100 °C, the initial stiffness of around 10–20 GPa is observed to increase by a factor of 2 or 3 within a few tens of hours [10–15].) It is also clear in Fig. 5 that data obtained by bend testing can be affected by curvature development, particularly at 1500 °C. Even slight curvature in the transverse direction is known to raise the apparent beam stiffness substantially and in those specimens the curvature was apparent to the naked eye. The origin of the curvature is not entirely clear, but it evidently arises from dimensional changes occurring during sintering (and is hence associated with grain boundary diffusion, rather than surface diffusion [17]). It is probably caused by different degrees of constraint along the edges of samples (compared with the interior), although it is possible that effects such as through-thickness gradients of microstructure (e.g. porosity level) could be at least partly responsible. It tends to be a problem only with relatively high sintering temperatures, such as those employed here. The forces generated are low, so the effect can be eliminated by the (small) weights used in the current work. (From an alternative point of view, the coatings creep very readily at these temperatures, and so can easily be flattened.) A problem does, however, arise with the overlaid weights, in that they tend to sinter to the coatings after a while, even with the imposition of periodic quenching. The measurements with weights at 1500 °C therefore extend only up to 10 h. Stiffness values for longer times were obtained from the extrapolated curve shown in Fig. 5. The equation for this curve is

$$E = 12.5 + 34.9t^{0.20} \quad (3)$$

where E is in GPa and t is in hours.

4. Spallation behaviour

4.1. Spallation lifetimes

Spallation results obtained for 1500 °C are summarized in Fig. 6, which presents data from 18 YSZ/alumina specimens, with coating thicknesses in the approximate range of 300–700 μm . The lifetimes, which do not include time spent during heating or cooling, range from ~ 40 to >150 h. It can be seen that, in general, thicker coatings show a distinct tendency to spall more quickly. This effect of coating thickness is perfectly intuitive (being due to the greater stored elastic strain energy, per unit area of interface), and is familiar for a wide range of coating types and environments. Nevertheless, these results do illustrate

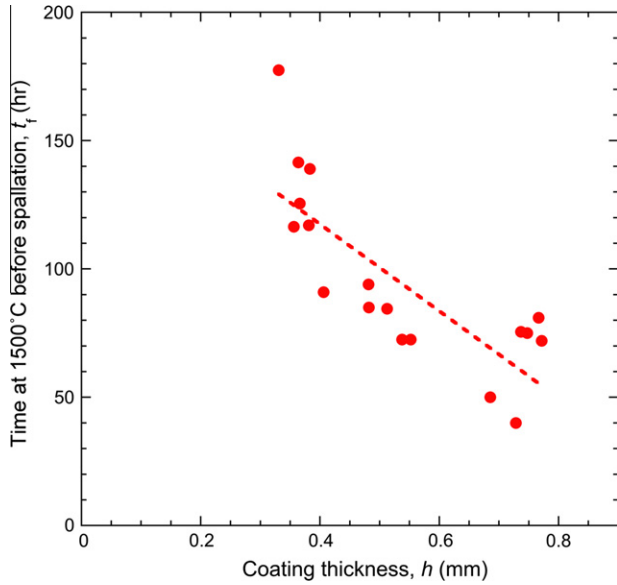


Fig. 6. Experimentally observed spallation lifetimes at 1500 °C for YSZ coatings on alumina substrates, plotted as a function of coating thickness.

quite clearly that any lifing methodology focused solely on the interface, or near-interface, regions (as are many previously proposed methodologies) is unlikely to be reliable.

4.2. Edge relaxation effects

In principle, for each of the spallation lifetimes shown in Fig. 6, it should be possible, using the corresponding coating stiffness value (E_{TBC}), to obtain a value for G_{ic} from Eq. (2). However, there is a complication associated with the in-plane dimensions of the specimens, which are rather small relative to the coating thickness, and also with the pronounced tendency for through-thickness (“segmentation”) cracks to form within them – as indeed commonly occurs in YSZ coatings on gas turbine components.² This can lead to “partial spallation”, commonly in the form of debonding and detachment of sections of the coating between a segmentation crack and the edge of the sample. Samples illustrating this effect are shown in Fig. 7. All such (substantial) debonding events tended to be classified as spallation (when viewed via the webcam), but careful characterization was then needed in order to apply an (energy-based) analysis, taking account of the relatively small area of many of the debonded regions – such that a significant fraction of the spalled material was close to either a crack or the edge.

Within regions of the coating close to segmentation cracks, or to specimen edges, the stresses responsible for

² Such through-thickness cracks are presumably created primarily by in-plane tensile stresses. With a conventional Ni alloy substrate, these arise (from differential thermal expansion) during the heating part of the cycle. With an alumina substrate, on the other hand, such stresses would be tensile only during cooling. Nevertheless, segmentation cracks appear to form readily in both cases. Furthermore, they appear to persist through prolonged holding at high temperature, suggesting that they commonly become too wide to readily be “healed” during such periods.

spallation become partially relaxed and a correction is required to account for this effect. At such a lateral free surface, the in-plane stress in the coating normal to that plane (which would be the one driving an interfacial crack from this region) must fall to zero. There will be a characteristic distance, δ , on moving away from the free surface, over which this stress rises to the far field value. The assumption is now made that this stress rises linearly from zero at the edge to σ_0 at a distance δ away from it

$$\begin{aligned} \sigma(x) &= \sigma_0 \left(\frac{x}{\delta} \right) & \text{for } x \leq \delta \\ \sigma(x) &= \sigma_0 & \text{for } x \geq \delta \end{aligned} \quad (4)$$

Assuming linear elastic behaviour, with an equal biaxial stress state, the stored elastic energy, U , associated with one of the two in-plane stresses (the one driving crack growth) can be expressed as

$$U = \frac{1}{2} \text{stress} \times \text{strain} \times \text{volume} = \frac{(1 - \nu \sigma^2)}{2E} \times \text{volume} \quad (5)$$

so that the energy in a relaxed region near a free edge may be written

$$\begin{aligned} U_{\text{edge}} &= \frac{1 - \nu}{2E} \int_0^\delta \sigma(x)^2 h w dx = \frac{h w (1 - \nu)}{2E} \int_0^\delta \frac{\sigma_0^2 x^2}{\delta^2} dx \\ &= \frac{h w (1 - \nu) \sigma_0^2}{2E \delta^2} \left[\frac{x^3}{3} \right] \end{aligned} \quad (6)$$

where w is the width of the region concerned. Equating this width to L , the (measured) perimeter of the relaxed region, leads to the following expression

$$U_{\text{edge}} = \frac{\sigma_0^2 L h \delta (1 - \nu)}{6E} \quad (7)$$

The stored elastic energy in regions remote from the edge and the segmentation cracks is given by

$$U_{\text{bulk}} = \frac{\sigma_0^2 (1 - \nu)}{2E} (A_f - L h \delta) \quad (8)$$

where A_f is the total interfacial area. Hence the total energy stored is given by

$$\begin{aligned} U_{\text{tot}} &= \frac{\sigma_0^2 (1 - \nu)}{6E} (L h \delta) + \frac{\sigma_0^2 (1 - \nu)}{2E} (A_f h - L h \delta) \\ &= \frac{h \sigma_0^2 (1 - \nu)}{2E} \left(A_f - \frac{2L \delta}{3} \right) \end{aligned} \quad (9)$$

The interfacial strain energy release rate is obtained on dividing this expression by A_f . Comparing the resultant expression with Eq. (2) reveals that the net effect is to introduce a correction factor accounting for stress relaxation effects, which reduces the driving force somewhat.

$$G_i = \frac{h E (\Delta \alpha \Delta T)^2}{2(1 - \nu)} \left(1 - \frac{2L \delta}{3A_f} \right) \quad (10)$$

The value of δ cannot be obtained rigorously, but its magnitude is expected to be of the order of h , the coating thickness – this follows, at least approximately, from St.

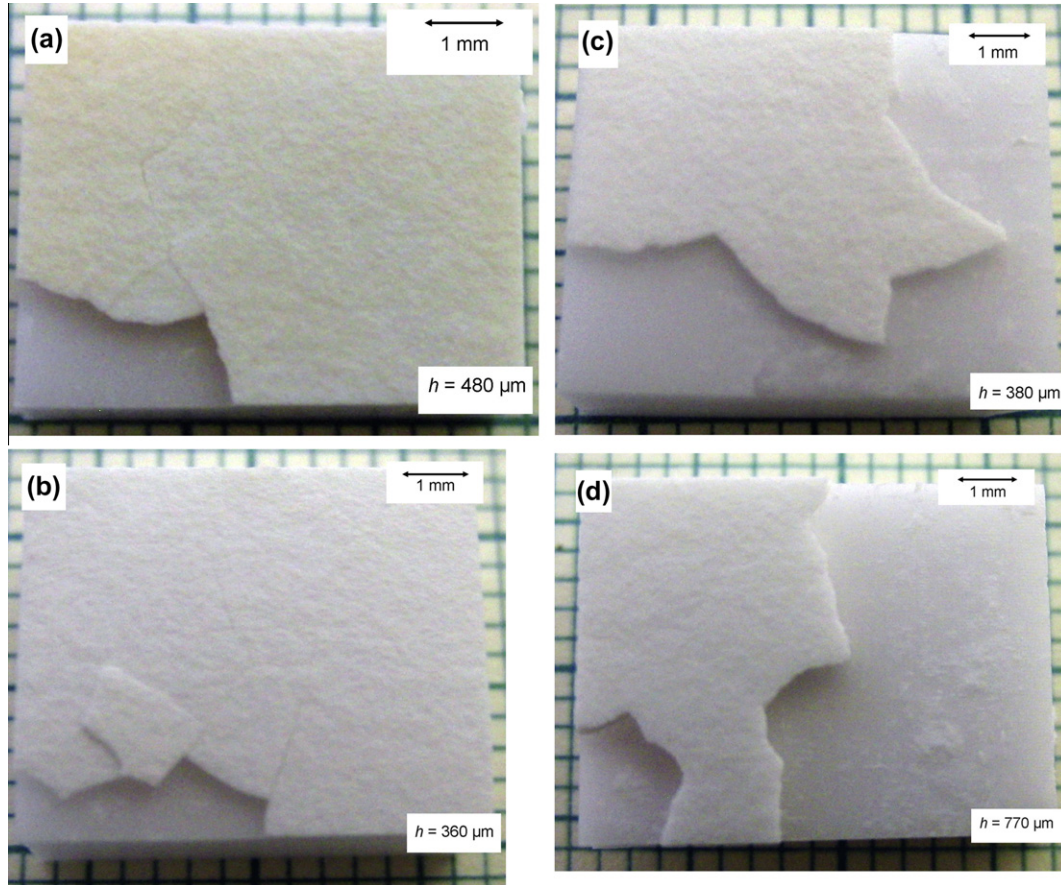


Fig. 7. Optical photographs of 4 YSZ/alumina samples after heat treatment at 1500 °C, showing partial coating spallation.

Venant's Principle – and this assumption was made in the current work. Values of A_f and L were measured by image analysis of the spalled specimens, applying ImageJ software to micrographs such as those shown in Fig. 7. The correction factor of $(1 - 2L\delta/(3A_f))$ had a value in the range of 30–70% for these specimens, depending on the size of the spalled region.

4.3. Deduction of interfacial fracture energies

For each of the spallation specimens,³ estimates of the critical strain energy release rate (G_{ic}) were obtained by substituting measured values of A_f and L into Eq. (3), together with the estimated misfit strain (2.2 millistrain) and the Young's modulus value corresponding to the heat treatment concerned (Fig. 5). The outcome of this operation is shown in Fig. 8. It can be seen that, while there is

certainly some scatter in the data, the results are consistent with an approximately constant value of G_{ic} , having a magnitude of the order of 300 J m^{-2} . This is encouraging, since it might be expected that the (YSZ/alumina) interface would not undergo much microstructural change, even when exposed to temperatures as high as 1500 °C, leading to an approximately constant value of G_{ic} .

It is also worth noting that this G_{ic} value represents a relatively tough interface. This is consistent with it having a rough topography (as a result of the laser treatment) and intimate contact having been achieved between the two constituents (via the use of VPS for the spraying). If the interface had been less tough, then presumably debonding would have occurred more readily – i.e. without requiring these relatively long times at high temperatures – but in such cases it was found that at least partial debonding tended to occur during spraying or shortly afterwards.

5. Conclusions

The following conclusions can be drawn from this work.

- (a) A straightforward methodology has been outlined for prediction of the spallation lifetimes of (plasma-sprayed) YSZ coatings, based on a simple (global) fracture mechanics criterion. This criterion

³ There are fewer data points in Fig. 8 than in Fig. 6 because, for some specimens, the heat treatment (including periodic quenching) was not terminated until it had continued well beyond the initial spallation event: the spallation lifetime (Fig. 6) for such specimens had been captured on video, but the repeated subsequent exposure to cooling jets caused the coatings to disintegrate, so the image analysis needed to implement Eq. (3) could not be carried out and the corresponding points could not be included in Fig. 8.

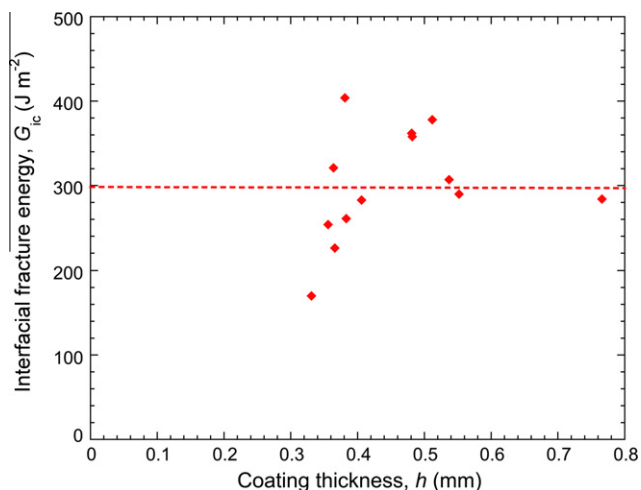


Fig. 8. Interfacial fracture energy values, plotted as a function of coating thickness: these data were obtained using Eq. (3), the spallation lifetime data in Fig. 6, the misfit strain during quenching ($\Delta\alpha\Delta T \sim 2.2$ millistrain) and measured values of A_f and L for the coating concerned.

is essentially the strain energy release rate associated with debonding reaching a critical value (the fracture energy of the interface), with this driving force being generated by the thermal misfit strain ($\Delta\alpha\Delta T$) associated with cooling (from a stress-free state at elevated temperature). It can often be assumed that all of this misfit strain is accommodated in the coating, making it easy to estimate the associated stresses and strain energy. The cooling may in practice not be entirely elastic, depending on the cooling rate, but in cases where some stress relaxation occurs it should be possible to establish an effective temperature drop and hence an effective misfit strain.

- (b) Under the proposed rationale, the key degenerative process is stiffening of the coating, as a consequence of sintering phenomena taking place at elevated temperature. This increase in stiffness leads to a higher strain energy release rate for a given misfit strain. (There is therefore particular concern about effects that might accelerate this sintering, such as the ingestion and absorption of certain CMAS species.) In practice, other degenerative processes, such as microstructural changes in the interfacial region, which might reduce the interfacial toughness, may simultaneously occur and it is difficult to make universal statements about the significance of such phenomena relative to sintering-driven increases in stiffness and hence in the strain energy release rate during cooling.
- (c) The outcome of an experimental investigation is also presented in this paper, designed to isolate the effects of sintering from those associated with changes in interfacial microstructure or other interactions between coating and substrate, and also to avoid any effects arising from thermal gradients in the system. This was achieved by using (fully dense) alumina substrates, allowing isothermal heat treatments (at

high temperatures) and ensuring that the interface remained essentially unchanged throughout. Misfit strains in this system on cooling to ambient temperature (of the order of a few millistrain) are similar in magnitude to those for conventional YSZ/superalloy combinations, although of opposite sign. Special processing procedures were developed, which created a suitably tough interface. It was also necessary to take account of edge effects and the influence of segmentation cracks on the effective strain energy release rate.

- (d) Experimental data were obtained for the coating stiffness as a function of heat treatment time and temperature. Spallation lifetime data at 1500 °C were also obtained, using a computer-controlled furnace system with a periodic quenching capability, for a substantial number of substrate/coating specimens, covering a range of coating thickness. A clear correlation was established between lifetime and coating thickness, as expected for debonding driven by release of stored strain energy (which is proportional to thickness). Furthermore, all of these spallation lifetimes were consistent with an approximately constant value of the interfacial fracture energy ($\sim 300 \text{ J m}^{-2}$).
- (e) The methodology presented here should be applicable to conventional coating systems. Of course, there are several complicating issues in such systems. The interfacial region, which commonly incorporates a bond coat, could undergo microstructural changes (including the formation of pores, cracks, etc.) during service. Nevertheless, it should be possible to ascribe a fracture energy to the region and to have at least some idea of how the value of this might change with time. Account may also need to be taken of the presence of a through-thickness thermal gradient, although it seems likely that the thermal conditions during cooling are more important than those during normal operation (with rapid quenching likely to limit stress relaxation during cooling and hence to promote debonding). The formation of segmentation cracks, and the associated stress relaxation, may need to be taken into account. It is also important to recognize that the model incorporates certain assumptions, such as the coating being stress-free at elevated temperature and the focus being on crack propagation being energetically favourable, rather than on crack initiation or sub-critical crack growth. It may also be noted that certain practical points immediately follow from the rationale, such as the potential value of monitoring the stiffness of coatings during service, which could be done without much difficulty.

Acknowledgements

Funding for this work has come from a Schools Competition Act Settlement Trust (SCAST) Research Scholarship. The authors are very grateful to Kevin Roberts and

Keith Page, of the Department of Materials Science in Cambridge University, for their extensive help with technical aspects of the spraying and the periodic quenching furnace. The assistance of Prof. Bill O'Neill, and Dr. Martin Sparkes, of the Institute for Manufacturing in Cambridge University, with the laser processing of the alumina substrates, is also gratefully acknowledged.

References

- [1] Peters M, Leyens C, Schulz U, Kaysser WA. *Adv Eng Mater* 2001;3:193.
- [2] Pature N, Gell M, Jordan E. *Science* 2002;296:280.
- [3] Evans AG, Mumm DR, Hutchinson JW, Meier GH, Pettit FS. *Prog Mater Sci* 2001;46:505.
- [4] Clarke DR, Levi CG. *Annu Rev Mater Res* 2003;33:383.
- [5] Gleeson B. *J Propul Power* 2006;22:375.
- [6] Cao XQ, Vassen R, Stoeber D. *J Eur Ceram Soc* 2004;24:1.
- [7] Schulz U, Leyens C, Fritscher K, Peters M, Saruhan-Brings B, Lavigne O, et al. *Aerosp Sci Technol* 2003;7:73.
- [8] Chi W, Sampath S, Wang H. *J Am Ceram Soc* 2008;91:2636.
- [9] Cernuschi F, Lorenzoni L, Ahmaniemi S, Vuoristo P, Mäntylä T. *J Eur Ceram Soc* 2005;25:393.
- [10] Ahrens M, Lampenscherf S, Vassen R, Stover D. *J Therm Spray Technol* 2004;13:432.
- [11] Tsiapas SA, Golosnoy IO, Damani R, Clyne TW. *J Therm Spray Technol* 2004;13:370.
- [12] Thompson JA, Clyne TW. *Acta Mater* 2001;49:1565.
- [13] Choi SR, Zhu DM, Miller RA. *J Am Ceram Soc* 2005;88:2859.
- [14] Traeger F, Ahrens M, Vaßen R, Stöver D. *Mater Sci Eng A* 2003;358:255.
- [15] Pfeiffer C, Affeldt E, Göken M. *Surf Coat Technol* 2011;205:3245.
- [16] Golosnoy IO, Tsiapas SA, Clyne TW. *J Therm Spray Technol* 2005;14:205.
- [17] Cipitria A, Golosnoy IO, Clyne TW. *Acta Mater* 2009;57:980.
- [18] Cipitria A, Golosnoy IO, Clyne TW. *Acta Mater* 2009;57:993.
- [19] Golosnoy IO, Cipitria A, Clyne TW. *J Therm Spray Technol* 2009;18:809.
- [20] Bolot R, Qiao J-H, Bertrand G, Bertrand P, Coddet C. *Surf Coat Technol* 2010;205:1034.
- [21] Borom MP, Johnson CA, Peluso LA. *Surf Coat Technol* 1996;87:116.
- [22] Mercer C, Faulhaber S, Evans AG, Darolia R. *Acta Mater* 2005;53:1029.
- [23] Kramer S, Faulhaber S, Chambers M, Clarke DR, Levi CG, Hutchinson JW, et al. *Mater Sci Eng A* 2008;490:26.
- [24] Li L, Hitchman N, Knapp J. *J Therm Spray Technol* 2010;19:148.
- [25] Chen X. *Surf Coat Technol* 2006;200:3418.
- [26] Drexler JM, Gledhill AD, Shinoda K, Vasiliev AL, Reddy KM, Sampath S, et al. *Adv Mater* 2011;23:2419.
- [27] Qian G, Nakamura T, Berndt CC. *Mech Mater* 1998;27:91.
- [28] Balke H, Hofinger I, Hausler C, Bahr HA, Weiss HJ, Kirchhoff G. *Arch Appl Mech* 2000;70:193.
- [29] Patterson T, Orloff DI, Bloom F. *Math Comput Modell* 2002;35:165.
- [30] Evans AG, Hutchinson JW. *Surf Coat Technol* 2007;201:7905.
- [31] Théry PY, Poulain M, Dupeux M, Braccini M. *J Mater Sci* 2009;44:1726.
- [32] Evans HE. *Surf Coat Technol* 2011;206:1512.
- [33] Hutchinson JW, Evans AG. *Surf Coat Technol* 2002;149:179.
- [34] Vaidyanathan K, Jordan EH, Gell M. *Acta Mater* 2004;52:1107.
- [35] Khan AN, Lu J. *Surf Coat Technol* 2007;201:4653.
- [36] Helminiak MA, Yanar NM, Pettit FS, Taylor TA, Meier GH. *Surf Coat Technol* 2009;204:793.
- [37] Johnson CA, Ruud JA, Bruce R, Wortman D. *Surf Coat Technol* 1998;109:80.
- [38] Choi SR, Hutchinson JW, Evans AG. *Mech Mater* 1999;31:431.
- [39] Zhao H, Yu Z, Wadley HNG. *Surf Coat Technol* 2010;204:2432.
- [40] Guo DZ, Wang LJ. *Surf Coat Technol* 1992;56:19.
- [41] Begley MR, Mumm DR, Evans AG, Hutchinson JW. *Acta Mater* 2000;48:3211.
- [42] Vasinonta A, Beuth JL. *Eng Fract Mech* 2001;68:843.
- [43] Yamazaki Y, Schmidt A, Scholz A. *Surf Coat Technol* 2006;201:744.
- [44] Zhao Y, Shinmi A, Zhao X, Withers PJ, Van Boxel S, Markocsan N, et al. *Surf Coat Technol* 2012;206:4922.
- [45] Moon C-O, Lee S-B. *Oxid Metals* 1993;39:1.
- [46] Clyne TW. *Key Eng Mater* 1996;116/7:307.
- [47] Drory MD, Thouless MD, Evans AG. *Acta Metall* 1988;36:2019.
- [48] Hutchinson JW, Suo Z. *Adv Appl Mech* 1992;29:63.
- [49] Vaßen R, Giesen S, Stöver D. *J Therm Spray Technol* 2009;18:835.
- [50] Schlichting KW, Pature NP, Jordan EH, Gell M. *Mater Sci Eng* 2003;A342:120.
- [51] Wakui T, Malzbender J, Steinbrech RW. *Surf Coat Technol* 2006;200:4995.
- [52] Paul S, Cipitria A, Golosnoy IO, Clyne TW. *J Therm Spray Technol* 2007;16:798.